

GBT local and global buckling analysis of aluminium and stainless steel columns

Rodrigo Gonçalves^a, Dinar Camotim^{b,*}

^a *Escola Superior de Tecnologia do Barreiro, Polytechnic Institute of Setúbal, R. Stinville 14, 2830-114 Barreiro, Portugal*

^b *Civil Engineering Department, Instituto Superior Técnico, TU Lisbon, Av. Rovisco Pais, 1049-001 Lisbon, Portugal*

Received 10 March 2004; accepted 12 March 2004

Available online 2 June 2004

Abstract

A non-linear elastic Generalised Beam Theory (GBT) is formulated and used to investigate the buckling behaviour of aluminium and stainless steel thin-walled columns. The modifications that must be incorporated in the conventional GBT, in order to handle the material non-linearity, are addressed and particular attention is paid to the need to define the stability problem in terms of instantaneous elastic moduli. After validating the proposed GBT, by means of its application to compressed rectangular plates, the unique features and capabilities of the theory are illustrated through the presentation and discussion of results concerning C-section and RHS columns. Stress–strain laws of the Ramberg–Osgood type are used to model the uniaxial behaviour and both J_2 -flow and J_2 -deformation plasticity theories are implemented.

© 2004 Elsevier Ltd. All rights reserved.

Keywords: Generalised beam theory; Stability analysis; Local-plate buckling; Distortional buckling; Global buckling; Aluminium columns; Stainless steel columns

1. Introduction

The structural applications of aluminium and stainless steel members have experienced a fast growth in the last few years, mostly because these members exhibit several distinct advantages, namely high strength/weight ratios, corrosion resistance, pleasing appearance, ease of maintenance, fabrication versatility and, last but not least, increasingly competitive prices [1–3]. However, cost and aesthetic demands often lead to the choice of very slender thin-walled members, a feature which makes them highly susceptible to local (local-plate or distortional) and/or global buckling and must be adequately reflected in their design rules. Naturally, efficient

(safe and economic) member designs can only be achieved if all instability phenomena are well understood and accurately predicted.

Unlike carbon (mild) steel, aluminium and stainless steel alloys exhibit an elastic–plastic behaviour characterised by (i) the absence of a well-defined yield stress and (ii) a marked non-linear uniaxial stress–strain law (even prior to the 0.2% proof stress), which often includes a considerable amount of strain-hardening [1]. This form of material behaviour implies that members buckle (either in local-plate, distortional or global modes) mostly in the non-linear range. Since this means that one must solve problems involving the plastic bifurcation of elastic–plastic solids, it is worth recalling that such phenomenon (i) is fully governed by the *active* (instantaneous) elastic moduli and, in columns (uniformly compressed bars), (ii) always takes place at the onset of elastic unloading and under increasing load [4,5]. Thus, the bifurcation load of an elastic–plastic

* Corresponding author. Tel.: +351-21-8418403; fax: +351-21-8497650.

E-mail address: dcamotim@civil.ist.utl.pt (D. Camotim).

column may be determined through the analysis of its *hypoelastic* counterpart [6,7]. This means that it is indispensable to account for the evolution of the material 3-D non-linear constitutive relations along the column fundamental equilibrium path, a procedure requiring load incrementation during the pre-buckling stage.

The characterisation of an elastic–plastic constitutive relation involves specifying the material initial yield surface (elastic limit), the strain-hardening rule (yield surface evolution) and the flow rule (direction of the incremental plastic strain vector). Moreover, when dealing with bifurcation problems, one must be aware of the well-known “*plate buckling paradox*”, described by Hutchinson [7] as follows: “It was discovered that bifurcation loads calculated using the simplest flow theories of plasticity consistently overestimated buckling loads of plates and shells obtained in tests. Calculations based on the less respectable deformation theories of plasticity gave reasonably good agreement with test results”.

The local buckling of a thin-walled member can only be determined with accuracy if the cross-section deformations are properly taken into account. The traditional way to achieve this objective is resorting to computationally intensive numerical analyses, (i) performed by means of the finite element (FE) or finite strip (FS) methods and (ii) adopting fine meshes of 2-D (thin-shell or strip) elements to discretise the member [8–10]. It is fair to say that, in the context of *linear elastic* buckling analyses, the recently developed Generalised Beam Theory (GBT) formulations significantly altered this situation.

The original GBT formulation was derived by Schardt and his co-workers [11,12] and can be employed to perform linear (first-order) and stability/bifurcation analyses in thin-walled prismatic members made of linear elastic isotropic materials. Its innovative aspects are the following: (i) a systematic procedure to incorporate cross-section wall membrane and flexural deformations¹ into the classic prismatic thin-walled bar theory, thus leading to a “extended theory” that can capture both local and global (instead of only global) phenomena, and (ii) unique modal decomposition features, which make it possible to obtain rather elegant and clarifying solutions for a wide range of structural problems involving thin-walled members and plate assemblies (e.g., stiffened panels) [13,14]. Although Schardt derived first-order GBT for both open and closed-section thin-walled members [11], almost all the readily available second-order GBT applications con-

cern only the former case [12]. Indeed, up until very recently,² research work dealing with a second-order GBT for closed-section members could only be found in a few reports published by Schardt and his co-workers at the University of Darmstadt (in German) [13,18]. Moreover, it is worth noticing that Davies and his collaborators, who used GBT extensively to investigate the elastic buckling behaviour of cold-formed steel (open-section) profiles [19,20], played a major role in the dissemination of Schardt’s work among the english-speaking research community [21,22].³ In the past couple of years, Silvestre and Camotim developed novel GBT formulations for linear elastic open-section thin-walled members, which can be used to assess (i) the linear and buckling behaviour of arbitrarily orthotropic laminated plate FRP (fibre-reinforced plastic) profiles [23–25] and (ii) the post-buckling behaviour of cold-formed steel structural elements [26]. In all the above cases, GBT has been established as a valid and often advantageous alternative to fully numerical FE or FS analyses.

The aim of this work is to present the formulation, validate and illustrate the application and capabilities of a GBT that can be applied to analyse the buckling behaviour of thin-walled columns with open or closed cross-sections and made of non-linear elastic–plastic materials such as aluminium or stainless steel. After a brief review of the conventional GBT procedure, attention is focused on the description and discussion of the specific modifications that must be incorporated in order to handle the non-linear material behaviour. Next, attention is paid to the evaluation of the instantaneous elastic moduli, according to the well-known J_2 -flow and J_2 -deformation small strain theories of plasticity, and one also discusses the differences between them (responsible for the “plate buckling paradox” mentioned earlier). Then, mostly for validation purposes (there are exact analytical results available in the literature [27]), the developed GBT approach is applied to simply supported rectangular plates under uniform compression. Finally, numerical results concerning the local and global buckling behaviour of C-section and rectangular hollow section (RHS) simply supported columns are presented and discussed.⁴ The aluminium

² It should be mentioned that, during the last year, some work has also been reported on this subject (in English) [15–17].

³ The overwhelming majority of the publications on GBT authored by Schardt and his co-workers (e.g., research reports, conference papers or journal articles) are available only in German.

⁴ In the latter case, *linear elastic* results are compared with “exact” FEM values, as the authors are not aware of any validation study concerning GBT buckling analyses of closed-section members.

¹ Note that these are genuine folded-plate theory concepts.

and stainless steel uniaxial constitutive behaviour is modelled using stress–strain laws of the Ramberg–Osgood type and, due to the above “buckling paradox”, both J_2 -flow and J_2 -deformation plasticity theories are implemented [28].

2. GBT equations for non-linear elastic materials

2.1. Brief review of the conventional GBT

Performing a linear stability analysis by means of the conventional (linear elastic and isotropic) GBT comprises two main tasks, namely: (i) a *cross-section analysis* and (ii) a *member analysis*. Their main aspects are briefly reviewed next, as applied to a thin-walled member with an arbitrary open or closed cross-section ($u(y)$, $v(y)$, $w(y)$) are the cross-section mid-line displacements along the local x , y , z axes—see Fig. 1):

(i) Cross-section analysis

(1) *Open-sections* [11,23,25]. The cross-section is divided into wall segments, separated by natural and intermediate nodes, and its deformed configuration is approximated by a linear combination of displacement functions, which stem from the sequential imposition of “unit warping (u) and transverse (w) displacements” at the natural and intermediate nodes, respectively,⁵ and are determined following a systematic procedure that involves using Vlassov’s hypothesis (null membrane shear strains) and solving a statically indeterminate folded-plate problem. These displacement functions are then used to calculate the components of four fully populated GBT stiffness and geometric matrices. Finally, a special change of (function) coordinates, selected so that two (out of three) stiffness matrices become *diagonal*, makes it possible to identify the GBT deformation modes and to evaluate the cross-section modal mechanical and geometrical properties. The amplitudes of the various deformation modes are the cross-section d.o.f.

(2) *Unicellular closed-sections* [11,13]. Besides all the displacement functions used in open cross-section analysis, which are determined in a similar fashion, it is also necessary to consider an additional one, which accounts for the classic Bredt’s tor-

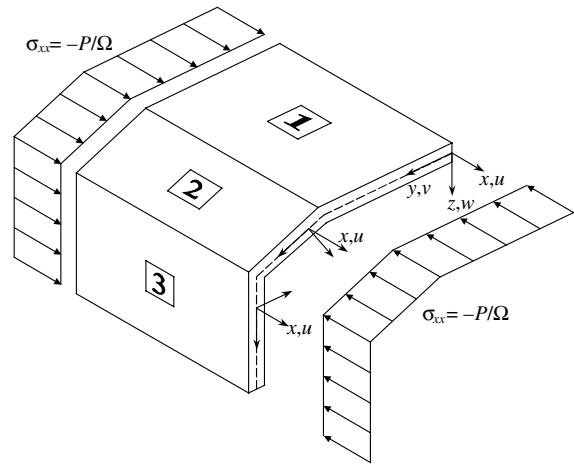


Fig. 1. Thin-walled column: geometry and local axes.

sion (e.g., [29]).⁶ This displacement function corresponds to the cross-section deformation due to a uniform shear flow, which means that wall membrane shear strains are involved and, thus, Vlassov’s assumption is not valid. It is obtained by imposing transverse displacements v , which are constant in each wall and must lead to a uniform shear flow. In general, transverse plate bending occurs and the flexural displacements are, once more, determined by solving a statically indeterminate folded-plate problem.

(ii) *Member analysis* (open and closed-sections) [12,24, 25]. Based on the cross-section modal mechanical and geometrical properties and the member length and end support conditions, one establishes a system of GBT differential equilibrium equations (one per deformation mode) and boundary conditions, which is expressed in terms of “amplitude functions” providing the longitudinal variation of the cross-section d.o.f. This system defines a standard eigenvalue problem and its solution, either analytical or numerical, yields the member bifurcation stress resultants (eigenvalues) and related buckling mode shapes (eigenfunctions).

2.2. Non-linear elastic materials

When dealing with non-linear elastic (hypoelastic) materials, both the cross-section and member analyses must be modified, mostly due to the need to determine the instantaneous elastic moduli. However, the bifurcation analysis simply consists of finding the fundamental

⁵ The free end nodes are treated as natural *and* intermediate nodes.

⁶ It is also possible to consider other “shear deformation modes”, for which Vlassov’s assumption is not valid. However, these modes are of no relevance for the problems dealt with in this work.

equilibrium states that have an “adjacent equilibrium configuration”. Such configuration must be located in the immediate vicinity of the fundamental (*stressed*) state and also satisfy a neutral equilibrium condition, expressed by means of the rate form of the principle of virtual work ⁷

$$\delta \dot{W} = \delta \dot{W}_E + \delta \dot{W}_I = 0, \tag{1}$$

where $\delta \dot{W}_E$ and $\delta \dot{W}_I$ are the member external and internal virtual work rates (note that, although the applications addressed in this work concern only *uniformly compressed* structural elements, Eq. (1) is quite general).

Since all column fundamental states exhibit uniform applied stress distributions $\sigma_{xx} = -P/\Omega$ (compressive axial load P and cross-section area Ω), the associated external and internal virtual work rates read (see Fig. 1),

$$\begin{aligned} \delta \dot{W}_E &= \int_V \sigma_{xx} \delta \dot{u}_{,x} dV = - \int_V \frac{P}{\Omega} \delta \dot{u}_{,x} dV, \\ \delta \dot{W}_I &= - \int_V (\sigma_{ij} + \dot{\sigma}_{ij}) \delta \dot{\epsilon}_{ij} dV \\ &= - \int_V \left(- \frac{P}{\Omega} \delta \dot{\epsilon}_{xx}^M + \dot{\sigma}_{ij} \delta \dot{\epsilon}_{ij} \right) dV, \end{aligned} \tag{2}$$

where the comma indicates differentiation, σ_{ij} are the fundamental state stress components ($\sigma_{xx} = -P/\Omega$ is the only non-null one), $\dot{\sigma}_{ij}$ are the stress-rate components, related to the strain-rate ones $\dot{\epsilon}_{ij}$ through the instantaneous elastic moduli, $\delta \dot{\epsilon}_{ij}$ are strain-rate component variations and the membrane axial strain-rate variation is given by

$$\delta \dot{\epsilon}_{xx}^M = \delta \dot{u}_{,x} + \delta (\dot{v}_x^2 + \dot{w}_x^2)/2. \tag{3}$$

After incorporating (2) and (3) into (1), one obtains,

$$\begin{aligned} \delta \dot{W} &= - \int_V \frac{P}{\Omega} \delta \dot{u}_{,x} dV - \int_V \left(- \frac{P}{\Omega} \delta \dot{\epsilon}_{xx}^M + \dot{\sigma}_{ij} \delta \dot{\epsilon}_{ij} \right) dV \\ &= \int_V \left(\frac{P}{\Omega} \frac{\delta (\dot{v}_x^2 + \dot{w}_x^2)}{2} - \dot{\sigma}_{ij} \delta \dot{\epsilon}_{ij} \right) dV = 0, \end{aligned} \tag{4}$$

a rate form of the principle of virtual work providing the means to detect adjacent equilibrium states in hypo-elastic columns.

Since the cross-section wall elements are subjected to uniaxial stress at any fundamental equilibrium state, the incremental stress–strain relations are of the form

$$\begin{aligned} \begin{Bmatrix} \dot{\sigma}_{xx}^B \\ \dot{\sigma}_{yy}^B \\ \dot{\sigma}_{xy}^B \end{Bmatrix} &= \begin{bmatrix} \dot{E}_{11} & \dot{E}_{12} & 0 \\ \dot{E}_{21} & \dot{E}_{22} & 0 \\ 0 & 0 & \dot{E}_{33} \end{bmatrix} \begin{Bmatrix} \dot{\epsilon}_{xx}^B \\ \dot{\epsilon}_{yy}^B \\ \dot{\epsilon}_{xy}^B \end{Bmatrix}, \\ \dot{\sigma}_{xx}^M &= E_T \dot{\epsilon}_{xx}^M, \end{aligned} \tag{5}$$

⁷ In this work, “rate” and “increment” are equivalent designations.

where \dot{E}_{ij} are the instantaneous elastic moduli, E_T is the uniaxial (longitudinal) tangent modulus and the superscripts ^(B) and ^(M) identify bending and membrane terms. Introducing the constitutive relations (5) into (4), one is led to the GBT equilibrium equations and boundary conditions (eigenvalue problem) [12,24]

$$\mathbf{C}\{\dot{\phi}_{,xxx}\} - \mathbf{D}\{\dot{\phi}_{,xx}\} + \mathbf{B}\{\dot{\phi}\} + \mathbf{P}\mathbf{X}^\textcircled{1}\{\dot{\phi}_{,xx}\} = \{0\}, \tag{6}$$

$$\begin{aligned} \{\delta \dot{\phi}_{,x}\}^T (\mathbf{C}\{\dot{\phi}_{,xx}\} + \mathbf{D}^\textcircled{2}\{\dot{\phi}\})|_0^L &= 0, \\ \{\delta \dot{\phi}\}^T (\mathbf{C}\{\dot{\phi}_{,xxx}\} + (\mathbf{D}^\textcircled{2} - \mathbf{D}^\textcircled{1} + \mathbf{P}\mathbf{X}^\textcircled{1})\{\dot{\phi}_{,x}\})|_0^L &= 0, \end{aligned} \tag{7}$$

where the components of vector $\{\dot{\phi}\}$ are functions providing the deformation mode amplitude rates (which combine to yield the buckling modes) and the GBT matrices \mathbf{C} , \mathbf{D} , \mathbf{B} and $\mathbf{X}^\textcircled{1}$ (geometric matrix associated to uniform compression) are now given by

$$\begin{aligned} C_{ij} &= C_{ij}^\textcircled{1} + C_{ij}^\textcircled{2} = \int_S t E_T u_i u_j dy + \int_S \frac{t^3}{12} \dot{E}_{11} w_i w_j dy, \\ D_{ij} &= D_{ij}^\textcircled{1} - D_{ij}^\textcircled{2} - D_{ji}^\textcircled{2} = \int_S \frac{t^3}{6} \dot{E}_{33} w_{i,y} w_{j,y} dy \\ &\quad - \int_S \frac{t^3}{12} \dot{E}_{12} (w_i w_{j,yy} + w_{i,yy} w_j) dy, \\ B_{ij} &= \int_S \frac{t^3}{12} \dot{E}_{22} w_{i,yy} w_{j,yy} dy, \quad X_{ij}^\textcircled{1} = \int_S \frac{t}{\Omega} (v_i v_j + w_i w_j) dy, \end{aligned} \tag{8}$$

with the integrations performed along the cross-section mid-line S . Note that all the above matrix components are *load-dependent*, through the instantaneous elastic moduli. One can solve Eqs. (6) and (7) either (i) for a given buckling load, determining the associated column length, or (ii) for a given column length, calculating the corresponding buckling load. In the first case, the solution is rather straightforward, as the active moduli at bifurcation are known a priori. In the second case, however, the load-dependence of the instantaneous moduli renders the solution considerably more difficult: it involves an iterative procedure and requires solving one eigenvalue problem per iteration.

For columns with pinned and free-to-warp end sections, combinations of deformation mode amplitude rate functions of the form

$$\dot{\phi}_k = \bar{\phi}_k \sin \left(\frac{m\pi x}{L} \right), \tag{9}$$

provide the exact eigenvalue problem solutions. The $\bar{\phi}_k$ values are the problem unknowns (participation factors of the various deformation modes in the column buckling mode), m is the buckling mode longitudinal half-wave number and L is the column length. If only a single deformation mode (k) is considered, the buckling stress, obtained from Eqs. (6) and (9), is given by

$$\sigma_{cr,k} = \frac{1}{X_{kk}^{\text{①}} \Omega} \left[C_{kk} \left(\frac{m\pi}{L} \right)^2 + D_{kk} + B_{kk} \left(\frac{L}{m\pi} \right)^2 \right], \quad (10)$$

This expression is quite interesting, as it clearly shows that, as L increases, the relevance of C_{kk} and B_{kk} for the value of $\sigma_{cr,k}$ changes in *opposite* ways: decreases in the first case and increases in the second [12].

3. Constitutive relations

3.1. J_2 -flow and J_2 -deformation theories

In this work, the \dot{E}_{ij} values are determined according to the rate form of isotropic small strain J_2 (von Mises) plasticity. Moreover, due to the ‘‘plate plastic buckling paradox’’ issue, both flow and deformation theories are implemented [28]. If the initial stress state is uniaxial, the \dot{E}_{ij} read, respectively for J_2 -flow [27] and J_2 -deformation [30] plasticity theories,

$$\begin{aligned} \dot{E}_{11} &= \frac{(A_T + 3)E_0}{(5 - 4\nu)A_T - (1 - 2\nu)^2}, \\ \dot{E}_{22} &= \frac{4A_T E_0}{(5 - 4\nu)A_T - (1 - 2\nu)^2}, \\ \dot{E}_{12} = \dot{E}_{21} &= \frac{(4\nu + 2A_T - 2)E_0}{(5 - 4\nu)A_T - (1 - 2\nu)^2}, \quad \dot{E}_{33} = 2G \end{aligned} \quad (11)$$

and

$$\begin{aligned} \dot{E}_{11} &= \frac{(A_T + 3A_S)E_0}{(2 + 3A_S - 4\nu)A_T - (1 - 2\nu)^2}, \\ \dot{E}_{22} &= \frac{4A_T E_0}{(2 + 3A_S - 4\nu)A_T - (1 - 2\nu)^2}, \\ \dot{E}_{12} = \dot{E}_{21} &= \frac{(4\nu + 2A_T - 2)E_0}{(2 + 3A_S - 4\nu)A_T - (1 - 2\nu)^2}, \\ \dot{E}_{33} &= \frac{2E_0}{2\nu - 1 + 3A_S}, \end{aligned} \quad (12)$$

where E_0 , G and ν are the initial uniaxial elastic modulus, shear modulus and Poisson’s ratio and one has $A_T = E_0/E_T$ and $A_S = E_0/E_S$ (E_S is the uniaxial secant modulus). Obviously, the values of both A_T and A_S depend on the applied stress (load) level and are obtained from a uniaxial stress–strain law that suitably describes the material behaviour along the fundamental path.

The use of the above rate constitutive relations makes it necessary to modify the standard GBT procedure. In fact, since the transverse displacements w of the column wall elements are determined by means of the force method, one must now use stiffness values K_{22} given by

$$K_{22} = \frac{t^3}{12} \dot{E}_{22}, \quad (13)$$

where t is the wall thickness. Of course, if $A_T = A_S = 1$ (linear elastic material), one gets the elastic plate bending stiffness $K_{22,el} = t^3 E_0 / 12(1 - \nu^2)$ (after using either (11) or (12)).

It is a well-established fact that flow and deformation plasticity theories exhibit major differences regarding the evolution of the \dot{E}_{ij} values along a uniaxial normal stress loading path [7]. The active shear modulus $\dot{G} = \dot{E}_{33}/2$ provides a classical illustration of these differences: while one has always $\dot{G} = G$ according to flow theory, the use of deformation theory leads to a vanishing \dot{G} , as A_S increases. Since the transverse stiffness K_{22} plays a key role in the GBT procedure, it is worth examining how the ratio $\eta = K_{22}/K_{22,el}$ evolves according to both theories:

- (i) *Flow theory.* η depends only on A_T and ν . For instance, if $\nu = 0.3$ one has $0.96 < \eta \leq 1$, which means that adopting $K_{22,el}$ instead of K_{22} leads to very small errors (regardless of the A_T value).
- (ii) *Deformation theory.* η depends on A_T , A_S and ν (A_T and A_S are dependent) and extremely small values can be attained (in sharp contrast with flow theory).

The curves shown in Fig. 2 provide a clear numerical illustration of the above η value differences. They concern a material behaviour characterised by a uniaxial stress–strain law of the Ramberg–Osgood type (see Eq. (14)) and the following parameter values: $E_0 = 70$ GPa, $\sigma_{0.2} = 200$ MPa, $\nu = 0.33$ and $n = 5$.

3.2. Uniaxial stress–strain law

As mentioned earlier, A_T and A_S are obtained from a suitable uniaxial stress–strain law. Up until a few years ago, the well-known Ramberg–Osgood expression [31]

$$\varepsilon = \frac{\sigma}{E_0} + 0.002 \left(\frac{\sigma}{\sigma_{0.2}} \right)^n, \quad (14)$$

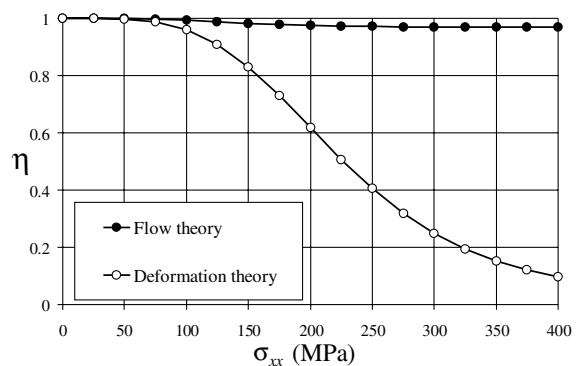


Fig. 2. Variation of η with σ_{xx} (longitudinal stress level).

where $\sigma_{0.2}$ is the 0.2% proof stress and n is the strain-hardening parameter, has been employed in virtually all the research work concerning aluminium or stainless steel structures. However, recent works by Hopperstad (see, e.g., [32]), for aluminium, and by Mirambell and Real [33] and Rasmussen [34], for stainless steel, have proposed alternative expressions, which are slightly more complicated but provide a much better fit of the experimental results throughout the whole stress range.

Although the vast majority of the numerical results presented in this work are based on uniaxial stress–strain laws of the Ramberg–Osgood type, the expression

$$\begin{cases} \varepsilon = \frac{\sigma}{E_0} + 0.002 \left(\frac{\sigma}{\sigma_{0.2}} \right)^n & \text{if } \sigma \leq \sigma_{0.2}, \\ \varepsilon = \frac{\sigma - \sigma_{0.2}}{E_{0.2}} + \varepsilon_u \left(\frac{\sigma - \sigma_{0.2}}{\sigma_u - \sigma_{0.2}} \right)^m + \varepsilon_{0.2} & \text{if } \sigma > \sigma_{0.2}, \end{cases} \quad (15)$$

where

$$\begin{aligned} E_{0.2} &= \frac{E_0}{1 + 0.002nE_0/\sigma_{0.2}}, & \varepsilon_{0.2} &= \frac{\sigma_{0.2}}{E_0} + 0.002, \\ \varepsilon_u &= 1 - \frac{\sigma_{0.2}}{\sigma_u}, & m &= 1 + 3.5 \frac{\sigma_{0.2}}{\sigma_u}, \\ \frac{\sigma_{0.2}}{\sigma_u} &= 0.2 + 185 \frac{\sigma_{0.2}}{E_0} & & \text{(austenitic and duplex alloys),} \\ \frac{\sigma_{0.2}}{\sigma_u} &= \frac{0.2 + 185\sigma_{0.2}/E_0}{1 - 0.0375(n-5)} & & \text{(all alloys),} \end{aligned} \quad (16)$$

proposed by Rasmussen [34], was also used to obtain RHS column results. This makes it possible to assess how the modelling of the uniaxial stress–strain curve affects the column local and global buckling behaviour.

4. Validation and illustrative examples

4.1. Rectangular plates

The buckling behaviour of simply supported rectangular aluminium plates, subjected to uniaxial uniform compression, was investigated by Handelman and Prager [27], who derived the analytical solution

$$\sigma_{cr} = \frac{\pi^2}{tb^2} \left[\frac{b^2 m^2}{a^2} K_{11} + 2K_{12} + \frac{a^2}{b^2 m^2} K_{22} \right], \quad (17)$$

$$\begin{aligned} K_{11} &= \frac{t^3}{12} \dot{E}_{11}, & K_{22} &= \frac{t^3}{12} \dot{E}_{22}, \\ K_{12} &= \frac{t^3}{12} (\dot{E}_{12} + \dot{E}_{33}), \end{aligned} \quad (18)$$

where t , a and b are the plate thickness, length and width and m is the buckling mode longitudinal half-wave number. It is interesting to note that the GBT solution given by Eq. (10), calculated for a deformation mode

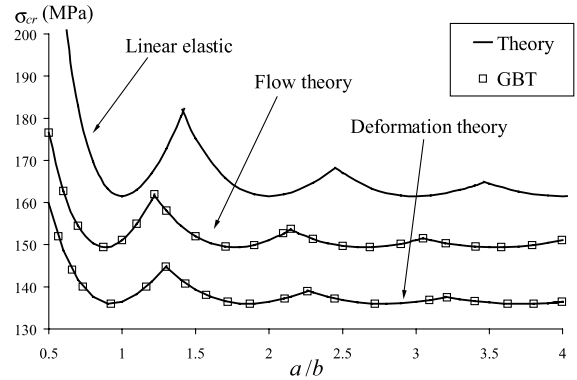


Fig. 3. Rectangular plate critical buckling stresses.

coinciding with the *exact* buckling mode ($u = v = 0$, $w = \sin(\pi y/b)$), is identical to Eq. (17).

Fig. 3 illustrates the critical stresses obtained by means of Eq. (17) and the proposed GBT formulation, for both J_2 -flow and J_2 -deformation plasticity theories. Also shown, for comparison purposes, are linear elastic values. These results concern plates with geometrical and material characteristics given by: $t = 2.5$ mm, $b = 100$ mm, $E_0 = 70$ GPa, $\sigma_{0.2} = 200$ MPa, $\nu = 0.33$ and $n = 5$ (low value, which corresponds to a markedly non-linear behaviour).

Only three equally spaced intermediate nodes were considered and, since the plate is simply supported along the four edges, the relevant GBT deformation modes exhibit only transverse displacements w , which satisfy the end conditions $w(0) = w(b) = 0$ (see Fig. 4). Note that, in this case, Eq. (6) are *uncoupled* and the critical buckling mode *always coincides* with deformation mode 1.

These results prompt the following remarks:

- (i) Because the elastic–plastic plates bifurcate in the non-linear range (although $\sigma_{cr} < \sigma_{0.2}$), there exists a considerable critical stress gap with respect to the linear elastic plates. Naturally, the largest differences occur for very short plates ($a/b < 1$).
- (ii) The results confirm that deformation theory leads to critical stress values lower than those obtained with flow theory [6].
- (iii) GBT provides virtually exact results with only three intermediate nodes. Moreover, the computational effort involved is significantly smaller than the one required by similar FE or FS analyses.

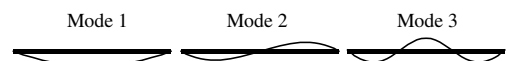


Fig. 4. GBT deformation modes for the rectangular plate.

4.2. C-section columns

Consider now the buckling behaviour of thin-walled C-section (lipped channel) columns with pinned and free-to-warp end sections and the cross-section dimensions given in Fig. 5. The material properties, corresponding to an aluminium alloy, are $E_0 = 70$ GPa, $\sigma_{0.2} = 200$ MPa, $\nu = 0.33$ and $n = 5$ (the same as in the previous example).

The cross-section has six natural nodes and seven additional auxiliary nodes were considered, namely three web intermediate nodes, one intermediate node per flange and one end node per lip. Then, the application of GBT leads to 13 orthogonal deformation modes: (i) the four rigid-body modes (extension ①, major ② and minor ③ axis bending and torsion ④), (ii) two distortional modes (⑤, ⑥) and (iii) seven local-plate modes. The first eight modes are the most relevant and their shapes are depicted in Fig. 6.

The buckling results obtained are shown in Figs. 7 (linear elastic behaviour), 8 (J_2 -flow theory) and 9 (J_2 -deformation theory). In each case, the curves plot bifurcation stresses σ_b associated with single half-wave mode

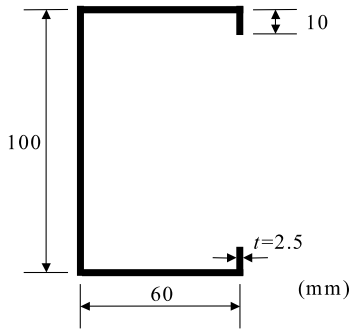


Fig. 5. C-section geometry.

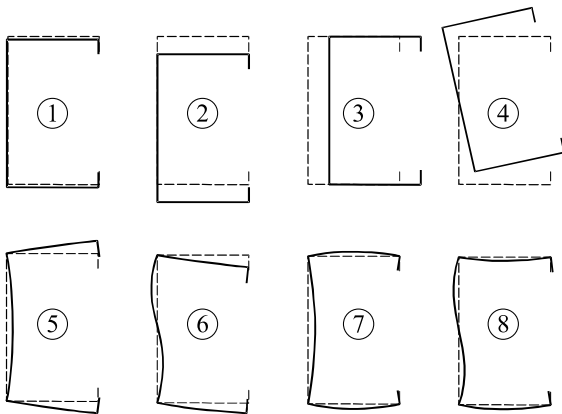


Fig. 6. C-section first eight deformation modes.

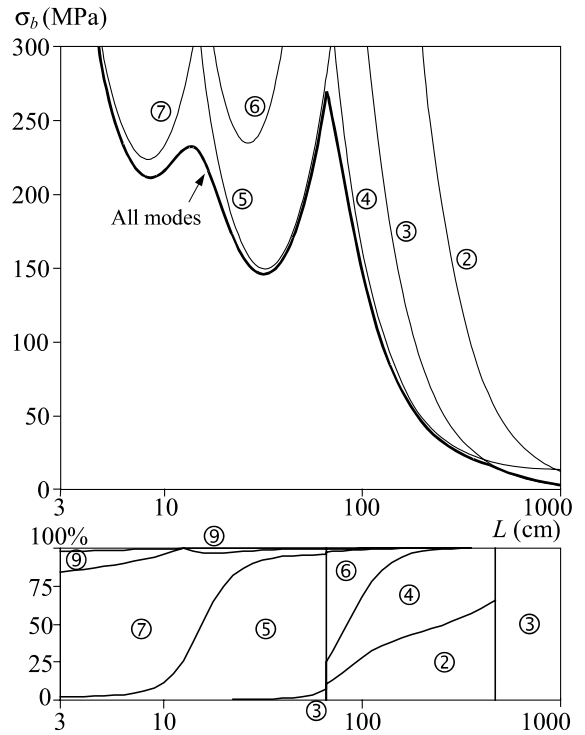


Fig. 7. C-section column linear elastic results.

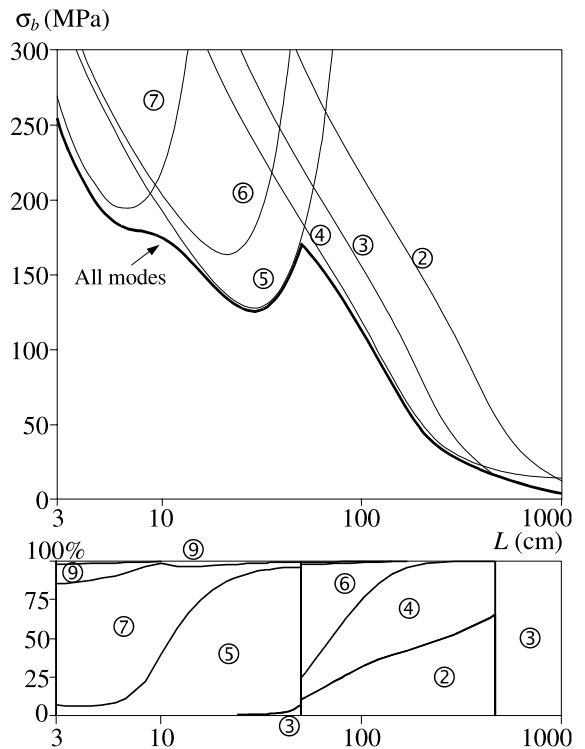


Fig. 8. C-section column elastic-plastic results (J_2 -flow).

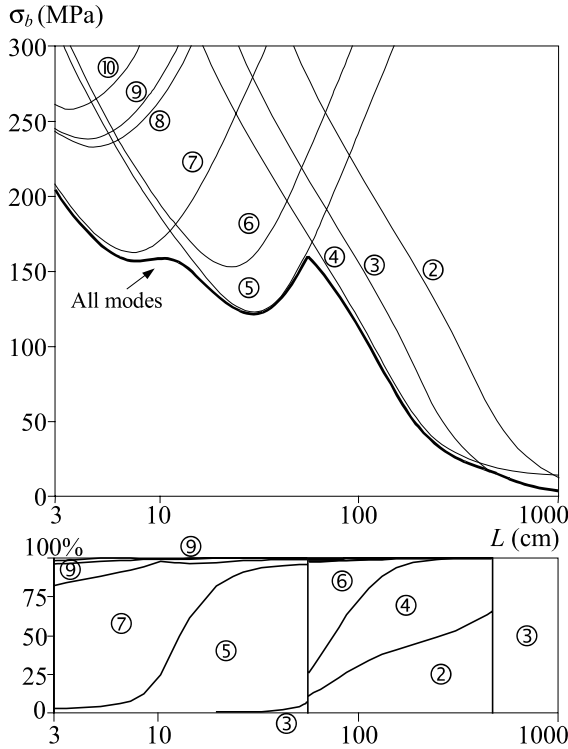


Fig. 9. C-section column elastic-plastic results (J_2 -deformation).

buckling (i) in individual GBT deformation modes (thin lines) and (ii) accounting for all GBT deformation modes (thick line). The lower diagrams supply the participation factors of each GBT deformation mode in the column buckling mode, thus providing an easy assessment of their relative importance. These diagrams constitute a unique GBT feature and provide a great help to visualise and characterise the column buckling mode shapes.

After observing the results presented in Figs. 7–9, the following conclusions can be drawn:

- (i) The results in Fig. 7 fully agree with those reported in the literature for cold-formed carbon steel columns [12,35]. According to their length value, the columns buckle in web-triggered local-plate modes ⑦ (very short columns), symmetric distortional modes ⑤ (short columns), mixed distortional–flexural–torsional modes ②+④+⑥ (intermediate columns), flexural–torsional modes ②+④ (long columns) or weak-axis flexural modes ③ (very long columns).
- (ii) The elastic–plastic bifurcation stresses (Figs. 8 and 9) are obviously lower than the elastic ones, except for very long columns, which buckle when $A_T \approx A_S \approx 1$. Smoother transitions between local-plate and distortional or distortional and global

buckling modes can be observed. As for the plates, deformation theory predicts significantly lower local bifurcation stresses than flow theory.

- (iii) Qualitatively, the flow theory individual distortional mode (⑤, ⑥) curves combine the deformation theory low negative slopes (left branches) with the linear elastic high positive slopes (right branches). Eq. (10) provides a clear explanation for this fact: while the descending (left) branches are governed by C_{kk}^1 ($C_{kk}^2 \approx 0$ for distortional modes), which is identical for flow and deformation theories (it depends on E_T), the ascending (right) ones are controlled by B_{kk} , which is very similar for the flow theory and linear elastic material models (it depends on K_{22}).
- (iv) The left branch of the flow theory individual local-plate mode ⑦ curve exhibits high slopes. Once more, Eq. (10) explains this behaviour: the controlling parameter is now C_{kk}^2 ($C_{kk}^1 \approx 0$ for local-plate modes), which varies much less than E_T (it depends on K_{11}).
- (v) The individual flexural (②, ③) and torsional (④) mode curves in Figs. 8 and 9 reproduce the results obtained with analytical tangent modulus formulae. Of course, for the torsional mode one must use $\bar{G} = \bar{E}_{33}/2$ (deformation theory) and $\bar{G} = G$ (flow theory).

Fig. 10 shows stress curves accounting for all GBT deformation modes and providing (i) single half-wave bifurcation stresses σ_b ($m = 1$ —dotted lines, identical to the thick curves of Figs. 7–9) and (ii) critical stresses σ_{cr} , corresponding to minimum values with respect to the half-wave number m (“all m ”—solid lines). These results

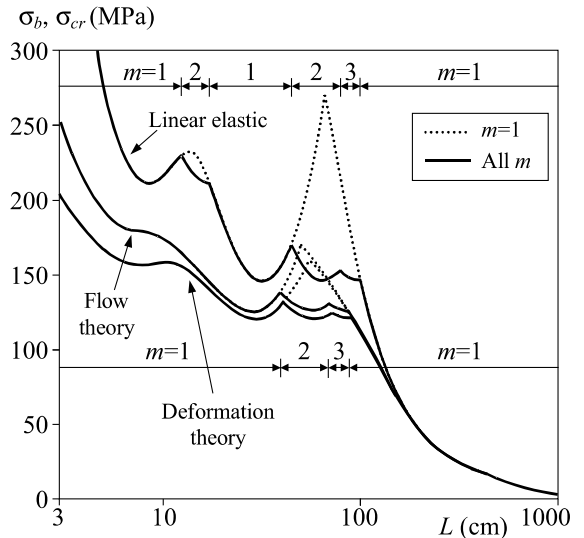


Fig. 10. C-section column critical stresses.

show that critical modes with $m > 1$ occur only for column lengths associated with transitions between (i) local-plate and distortional modes (linear elastic behaviour) and (ii) distortional and flexural-torsional modes (all behaviours).

4.3. RHS columns

Finally, one addresses the buckling behaviour of RHS columns with pinned and free-to-warp end sections and the cross-section dimensions shown in Fig. 11. The material data concerns now a stainless steel alloy and reads $E_0 = 200$ GPa, $\nu = 0.3$, $\sigma_{0.2} = 300$ MPa and $n = 5$.

The cross-section discretisation involves 4 natural and 10 intermediate nodes (3 per web and 2 per flange), leading to 15 deformation modes: extension ①, minor ② and major ③ axis bending, torsion ④, distortion ⑤ and 10 local-plate modes. Fig. 12 displays the shapes of the first 10 of these deformation modes.

The results are shown in Figs. 13 (linear elastic), 14 (J_2 -flow theory) and 15 (J_2 -deformation theory). As for the C-section columns, the curves provide bifurcation stresses associated with $m = 1$ and buckling in individual modes (thin lines) or accounting for all modes (thick lines). Once again, the mode participation factor diagrams are shown below. Lastly, Fig. 16 supplies

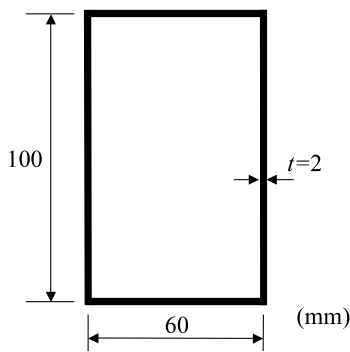


Fig. 11. RHS geometry.

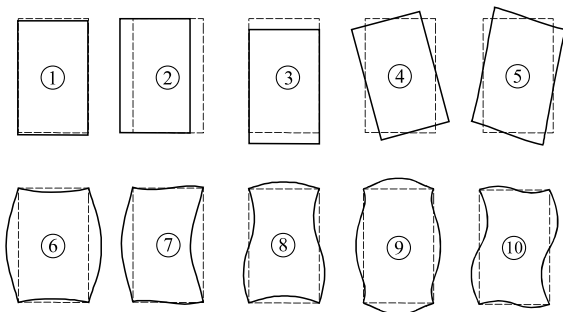


Fig. 12. First 10 RHS deformation modes.

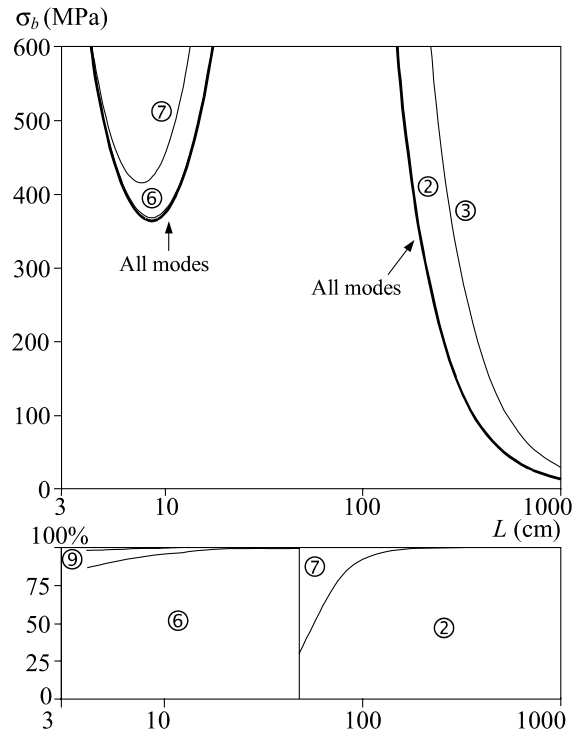


Fig. 13. RHS column linear elastic results.

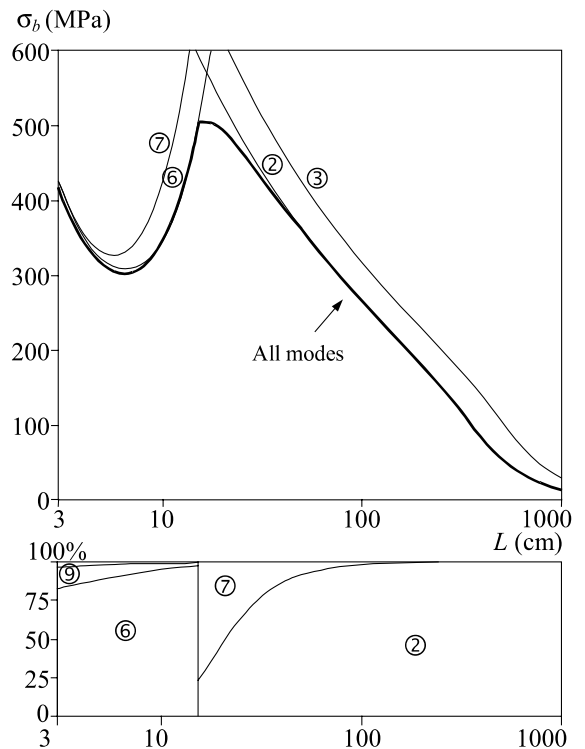


Fig. 14. RHS column elastic-plastic results (J_2 -flow).

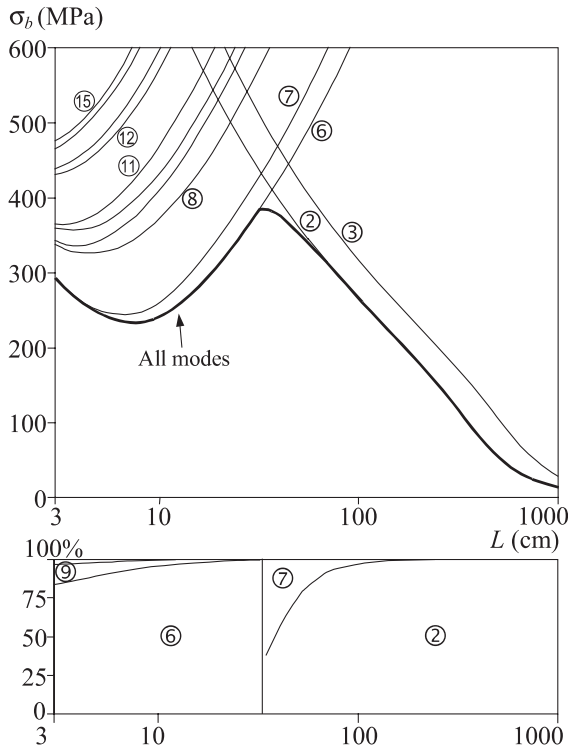


Fig. 15. RHS elastic-plastic column results (J_2 -deformation).

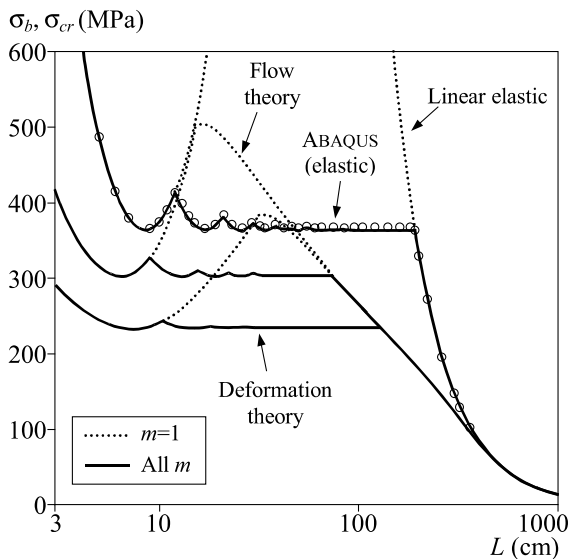


Fig. 16. RHS column critical stresses.

bifurcation ($m = 1$ —dotted lines) and critical (“all m ”—solid lines) stress values that take into account all GBT deformation modes. In order to check the validity of the GBT formulation for closed-section members, Fig. 16

includes also linear elastic critical stress values obtained with the FEM (identified by circles), using the code ABAQUS [36]. Four node shell (S4) finite elements were used to discretise the columns.

The interpretation of Figs. 13–16 leads to the following comments:

- (i) Since the linear elastic GBT and FEM critical stress values virtually coincide (errors below 1%), it seems fair to infer the validity of the developed GBT formulation for tubular thin-walled members [37].
- (ii) Given the high torsional stiffness of closed sections (particularly in comparison with open sections), the torsional ④ and distortional ⑤ modes never participate in the column buckling mode. This means that their removal from the GBT system (Eqs. (6) and (7)) does not affect the accuracy of the results, while leading to computational savings. One notes that the column buckling modes involve only flexural and local-plate modes. Indeed, Figs. 13–15 ($m = 1$) show that, depending on their length, the columns buckle in web-triggered symmetric local-plate modes ⑥ (short to intermediate columns), mixed anti-symmetric local-plate and flexural modes (⑦+②) (intermediate columns) or weak-axis flexural modes ② (long columns).
- (iii) As in the case of the C-section columns, one notices that the elastic-plastic σ_b values lie below the elastic ones (except for long columns $-A_T \approx A_S \approx 1$), J_2 -deformation theory leads to lower σ_b values, the individual flexural mode (②, ③) curves duplicate the results yielded by tangent modulus formulae and the transition between local-plate and global critical modes occurs for smaller σ_b values in either of the elastic-plastic cases.
- (iv) It is interesting to notice the presence of a much larger number of individual mode curves in Figs. 9 and 15 (J_2 -deformation) than in Figs. 8 and 14 (J_2 -flow). This is due to the very pronounced \dot{E}_{ij} value erosion associated with J_2 -deformation theory, which significantly lowers several higher-order local-plate curves, thus making them visible in the figures.
- (v) Qualitatively, the main difference between the “all m ” curves shown in Figs. 10 (C-section) and 16 (RHS) concerns the intermediate length range: the C-section columns buckle in two or three half-wave distortional modes, whereas the RHS ones buckle in local-plate modes with a fairly large number of half-waves.

4.3.1. Effect of the uniaxial stress-strain law

In order to assess the influence of the uniaxial stress-strain modelling on the column local and global buckling behaviour, Fig. 17 shows a comparison between the thick line curves given in Figs. 14 and 15 (single half-wave buckling—all modes) and similar bifurcation stress

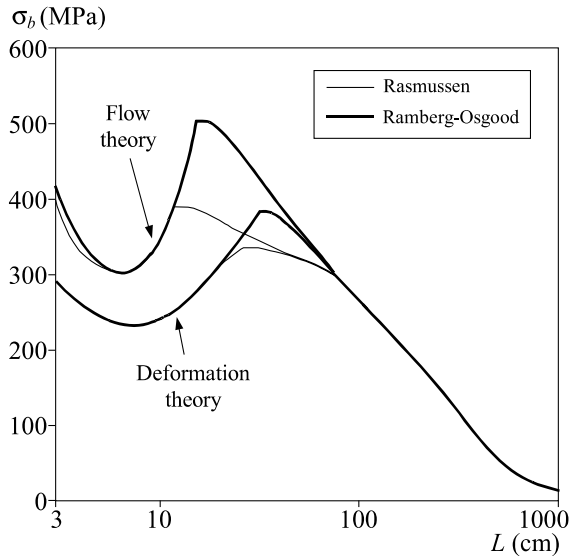


Fig. 17. Effect of uniaxial stress–strain law on the RHS column buckling behaviour (J_2 -flow and J_2 -deformation).

curves, based on the stress–strain law recently proposed by Rasmussen [34] (Eq. (15)), combined with the “all alloys” σ_u expression given in Eq. (16).

Recalling that the two stress–strain laws differ only for $\sigma > \sigma_{0.2} = 300$ MPa (in this particular case), one observes that the use of Rasmussen’s law only alters (lowers) the single half-wave buckling stresses of columns with intermediate lengths. Moreover, since the minimum local-plate buckling stresses remain virtually unchanged (for both plasticity theories), it possible to guarantee that the “all m ” curves displayed in Fig. 16 would not be affected by the uniaxial stress–strain law change.

5. Conclusions

A non-linear elastic generalised beam theory was formulated, validated and used to investigate the local and global buckling behaviour of open and closed thin-walled columns made of non-linear elastic–plastic materials, such as aluminium and stainless steel alloys.

Following a very brief review of the conventional GBT procedure, the modifications required to handle the non-linear material behaviour were described and discussed in detail. Special attention was devoted to the implications of using the active elastic moduli predicted by deformation and flow plasticity theories. In order to obtain the numerical results presented in the paper, both the well-known J_2 -deformation and J_2 -flow small strain plasticity theories were implemented. The material uniaxial constitutive relation was modelled by means of Ramberg–Osgood laws (almost always) and also a

compound stress–strain law recently proposed by Rasmussen.

For validation purposes, the proposed GBT formulation was used to determine the buckling behaviour of simply supported uniformly compressed rectangular plates. The comparison with exact analytical values available showed that GBT provides extremely accurate results with a rather small computational effort.

Finally, in order to illustrate the application and capabilities of the GBT approach, the numerical results of an investigation on the local and global buckling behaviour of C-section (aluminium) and RHS (stainless steel) simply supported columns were presented and discussed. Among the conclusions drawn from this study, the following deserve to be emphasised:

- (i) The proposed non-linear GBT constitutes an efficient tool to investigate the local and global buckling behaviour of aluminium and stainless steel columns. When compared with FE or FS analyses, it provides equally accurate and much more comprehensive results, while involving a considerably smaller computational effort.
- (ii) As expected, in view of the well-known “plate plastic buckling paradox”, both the distortional (C-section) and, mostly, the local-plate (C-section and RHS) column buckling stresses obtained using the J_2 -deformation and J_2 -flow plasticity theories differ considerably. If one wants to reach safe and economic design rules, it is essential to shed new light on this matter. This will certainly require a comparison between numerical and (carefully obtained) experimental results.
- (iii) For stainless steel RHS columns, the effect of the uniaxial stress–strain modelling was assessed through the comparison of buckling stresses obtained using a classic Ramberg–Osgood law and Rasmussen’s compound law. Although the differences were not too relevant for the particular cross-section geometry and material properties dealt with here, it became clear that this would not always be the case. This issue requires further study (both for stainless steel and aluminium columns).

Finally, just two words to mention that the authors are currently working on an extension of this GBT approach, aimed at assessing the buckling behaviour of members acted by *arbitrary* applied stress distributions.

References

- [1] Galambos TV, editor. Guide to stability design criteria for metal structures. New York: John Wiley & Sons; 1998.
- [2] Mazzolani F. Design criteria for aluminium structures: technology, codification and application. In: Mazzolani F,

- editor. Aluminium Structural Design (CISM Course 443). Wien: Springer-Verlag; 2002. p. 1–87.
- [3] Nethercot D, Gardner L. Exploiting the special features of stainless steel in structural design. In: Chan SL, Teng JC, Chung KF, editors. Advances in steel structures (ICASS'02—Hong Kong, December 9–11), vol. 1. Amsterdam: Elsevier; 2002. p. 43–55.
 - [4] Shanley FR. Inelastic column theory. *J Aeronaut Sci* 1947;14:261–8.
 - [5] Hill R. A general theory of uniqueness and stability in elastic–plastic solids. *J Mech Phys Solids* 1958;6:236–49.
 - [6] Tvergaard V, Needleman A. On the foundations of plastic buckling. In: Rhodes J, Walker AC, editors. Developments in thin-walled structures—1. London: Elsevier Applied Science; 1982. p. 205–33.
 - [7] Hutchinson JW. Plastic buckling. In: Yih CS, editor. Advances in applied mechanics, vol. 4. New York: Academic Press; 1974. p. 67–144.
 - [8] Rasmussen KJ. Numerical simulation and computational models in coupled instabilities. In: Rondal J, Dubina D, Gioncu V, editors. Coupled instabilities in metal structures (CIMS'96—Liège, September 5–7). London: Imperial College Press; 1996. p. 45–60.
 - [9] Sridharan S. Numerical simulation and computational models for coupled instabilities: general report. In: Camotim D, Dubina D, Rondal J, editors. Coupled instabilities in metal structures (CIMS'2000—Lisbon, September 21–23). London: Imperial College Press; 2000. p. 61–72.
 - [10] Mennink J. Cross-sectional stability of aluminium extrusions. PhD Thesis, Technische Univ Eindhoven, 2002.
 - [11] Schardt R. Verallgemeinerte technische biegetheorie. Berlin: Springer-Verlag; 1989 [in German].
 - [12] Schardt R. Generalised beam theory—an adequate method for coupled stability problems. *Thin-Walled Struct* 1994;19(2–4):161–80.
 - [13] Möller R. Zur berechnung prismatischer strukturen mit beliebigem nicht formtreuem querschnitt. Bericht Nr. 2, Institut für Statik der Technischen Hochschule Darmstadt, 1982 [in German].
 - [14] Schardt R, Heppner K-U, Neujahr M. Über die ermittlung eines schwingbeiwertes für prismatische brücken mit der verallgemeinerten technischen biegetheorie. *Bauingenieur* 1995;70:531–9 [in German].
 - [15] Simão P, Silva LS. Comparative analysis of the stability of open and closed thin-walled section members in the framework of generalised beam theory. In: Lamas A, Silva LS, editors. Proceedings of the Third European Conference on Steel Structures (EUROSTEEL'02—Coimbra, September 19–20), vol. I. 2002. p. 711–21.
 - [16] Simão P, Silva LS. Stability behavior of closed cross-section thin-walled prismatic members in the framework of generalized beam theory. In: Hancock GJ, Bradford MA, Wilkinson TJ, Uy B, Rasmussen KJ, editors. Advances in structures (ASSCCA'03—Sydney, June 23–25), vol. 1. Lisse: Balkema; 2003. p. 503–9.
 - [17] Camotim D, Gonçalves R. GBT-based local and global buckling analysis of C-section and RHS stainless steel columns. In: Stainless steel in structures (International Experts Seminar—Ascot, May 20). Ascot: The Steel Construction Institute; 2003. p. 81–92.
 - [18] Schardt R, Issmer H, Mörschardt S. Gesamtstabilität dünnwandiger Stäbe. Bericht Nr. 5, Institut für Statik der Technischen Hochschule Darmstadt, 1986 [in German].
 - [19] Leach P, Davies JM. An experimental verification of the generalised beam theory applied to interactive buckling problems. *Thin-Walled Struct* 1996;25(1):61–79.
 - [20] Davies JM. Generalised beam theory for coupled instability problems. In: Rondal J, editor. Coupled instabilities in metal structures: theoretical and design aspects, CISM Course 379, Part IV. Wien: Springer-Verlag; 1998. p. 151–223.
 - [21] Davies JM, Leach P. First-order generalised beam theory. *J Construct Steel Res* 1994;31(2–3):187–220.
 - [22] Davies JM, Leach P. Second-order generalised beam theory. *J Construct Steel Res* 1994;31(2–3):221–41.
 - [23] Silvestre N, Camotim D. First order generalised beam theory for arbitrary orthotropic materials. *Thin-Walled Struct* 2002;40(9):755–89.
 - [24] Silvestre N, Camotim D. Second order generalised beam theory for arbitrary orthotropic materials. *Thin-Walled Struct* 2002;40(9):791–820.
 - [25] Silvestre N, Camotim D. GBT buckling analysis of pultruded FRP lipped channel members. *Comput Struct* 2003;81(18–19):1889–904.
 - [26] Silvestre N, Camotim D. Non-linear generalised beam theory for cold-formed steel members. *Int J Struct Stability Dynam* 2003;3(4):461–90.
 - [27] Handelman GH, Prager W. Plastic buckling of a rectangular plate under edge thrusts. NACA TN 1530, 1948.
 - [28] Chen WF, Han D. Plasticity for structural engineers. New York: Springer-Verlag; 1988.
 - [29] Oden JT, Ripperger E. Mechanics of elastic structures. 2nd ed. Washington: Hemisphere Publishing; 1981.
 - [30] Bijlaard P. Theory and tests on the plastic stability of plates and shells. *J Aeronaut Sci* 1949;16:529–41.
 - [31] Ramberg W, Osgood WR. Description of stress–strain curves by three parameters, NACA TN 902, 1943.
 - [32] Moen LA, De Matteis G, Hopperstadt OS, Langseth M, Landolfo R, Mazzolani F. Rotational capacity of aluminium beams under moment gradient II: numerical simulations. *J Struct Eng* 1999;125(8):921–9.
 - [33] Mirambell E, Real E. On the calculation of deflections in structural stainless steel beams: an experimental and numerical investigation. *J Construct Steel Res* 2000;54(1):109–33.
 - [34] Rasmussen KJ. Full-range stress–strain curves for stainless steel alloys. *J Construct Steel Res* 2003;59(1):47–61.
 - [35] Silvestre N, Simão P, Camotim D, Silva LS. Application of GBT to the stability analysis of cold-formed steel members. In: Lamas A, Real PV, Silva LS, editors. Construção Metálica e Mista 3 (Aveiro, December 6–7), 2001, p. 617–26 [in Portuguese].
 - [36] Hibbit, Karlsson & Sorensen Inc. ABAQUS Standard, version 6.3-1. 2002.
 - [37] Gonçalves R, Camotim D, Dinis PB. Generalised beam theory to analyse the buckling behaviour of aluminium or steel open and closed thin-walled members. Proceedings of the 4th International Conference on Thin-Walled Structures (ICTWS 2004—Loughborough, June 22–24), 2004. (in press).